Machine Vision System Utilizing Black Silicon CMOS Camera for Through-Silicon Alignment

Aleksandr Andreevich Vlasov, Alp Eren Aydin, Topi Uusitalo, Jukka Viheriälä, and Mircea Guina, *Member, IEEE*

***Abstract*— Current development trends concerning miniaturizing of electronics and photonics systems are aiming at assembly and 3-D co-integration of a broad range of technologies including MEMS, microfluidics, wafer level optics, and silicon photonics. To this end, on-chip integration using silicon-photonics platform offers a wide range of possibilities addressing passive optics functionality, active optoelectronic devices, and compatibility with CMOS fabrication. On the other hand, the hybrid technology enabling volume manufacturing of such system-on-chip components, it is still in an early development stage. Here, a new type of machine vision system enabling precision stacking and bonding processes of III–V components on silicon photonics chips is introduced. In particular, we focus on the ability to see through substrates with high resolution, which is crucial for the alignment of the markers used for assembly of integrated components on silicon wafer. The system is based on the use of a black silicon enhanced CMOS sensor with extended wavelength response beyond transparency cutoff wavelength for silicon substrate. We study the use of the camera system as a microscope with bottom coaxial infrared (IR) illumination scheme and demonstrate the ability of through-silicon vision for one- and two-layered silicon photonic integrated circuit (PIC) samples. The ability of observing objects with dimensions down to 2 μm is confirmed. This resolution is close to diffraction limit and corresponds to the dimensions of optical waveguide structures on the PICs surface. In addition, we demonstrate the implementation of a 2-D Fourier transform-based autofocusing technique for through-silicon IR microscopy. These building blocks offer a solution for advanced photonic integration processes and other through-silicon vision-related applications, which is instrumental for a large variety of assembly, lithography, and wafer bonding setups.**

***Index Terms*— Assembly processes, infrared (IR) imaging, IR microscopy, laser-assisted bonding (LAB), machine vision, photonic integration, silicon devices, silicon photonics, through-silicon vision.**

I. Introduction

THE annual growth of data transfer rates linked to digitalization of the world economy, for example, in the form of artificial intelligence, Internet of Things (IoT), and large-scale machine-to-machine communication, requires a continuous development of infocommunication technology (ICT) infrastructure. Broadly speaking, the underlying technology is largely enabled by the miniaturization of electronics and photonics. In the field of photonics, the transition from bulk and fiber-optics to the chip level integrated photonic integrated circuits (PICs) enables a tremendous shrinking of photonic modules to a chip with the size comparable to a thumb nail—similar to the integrated electronics [1], [2], [3]. Nowadays, many of the photonic devices, such as transceivers, optical amplifiers, and gyroscopes, which existed as complex multi-component large instruments for a long time, are transitioning to high-density integrated embodiment with better characteristics [2], [3], [4].

To this end, advances toward full-scale wafer level assembly cover a wide range of topics with different integration levels, e.g., progressing from stacking of different chips, chip-to-wafer, and wafer-to-wafer bonding processes. The general aim is to maximize the parallelization of assembly process and to minimize wasted volume and material in order to reduce module cost and size. As general technology approaches supporting these developments, we should mention the rapid developments of transfer printing enabling co-integration of multiple devices from different starting wafers onto a common substrate [5], and the flip-chip bonding used for transferring of ready individual device chips to a common substrate or a more complex chip [6], [7].

Despite the availability of commercial approaches for hybrid integration involving thermo-compression bonding (TCB) and mass-reflow (MR) processes widely used in electronics, there is a need to develop more advanced tools addressing precise alignment of photonics components, faster assembly process, and in general, improved reproducibility and higher yield. To this end, laser-assisted bonding (LAB), which is known to be much faster than classical TCB and MR processes, is expected to meet the strict requirements of precise bonding processes as LAB cause negligible thermo-induced stress and warpage of the bonded surfaces (up to 3-4 times lower) [8], [9]. Yet another advantage is the fact that LAB can rely on solder surface tension-driven self-alignment [10], which can help to achieve better performance of photonic integration [9], [10], [11].

Generally speaking, the bonding processes require a machine vision system to provide means for accurate part manipulation prior to the bonding process. In numerous stacking operations, direct vision to bonding interfaces is obstructed by parts to be bonded. Similarly, postbond part inspection

Manuscript received 29 August 2022; revised 31 October 2022; accepted 23 November 2022. Date of publication 28 November 2022; date of current version 18 January 2023. This work was supported in part by Business Finland through project PICAP (Photonic Integrated Circuits for Industrial Applications) under Grant 44761/31/2020 and in part by the Academy of Finland through Photonics Flagship Program PREIN (Photonics REsearch and INnovation) under Grant #320168. Recommended for publication by Associate Editor K. Sakuma upon evaluation of reviewers' comments. *(Corresponding author: Aleksandr Andreevich Vlasov.)*

The authors are with the Optoelectronics Research Centre, Physics Unit, Tampere University, 33720 Tampere, Finland (e-mail: aleksandr.vlasov@tuni.fi; alp.aydin@tuni.fi; topi.uusitalo@tuni.fi; jukka.viheriala@tuni.fi; mircea.guina@tuni.fi).

This article has supplementary material provided by the authors and color versions of one or more figures available at https://doi.org/10.1109/TCPMT.2022.3225051.

Digital Object Identifier 10.1109/TCPMT.2022.3225051

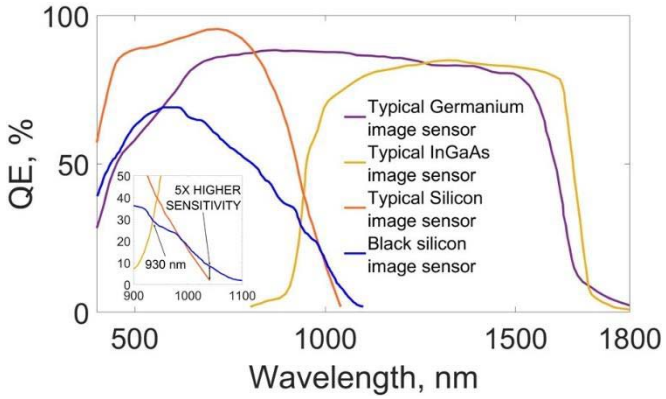

Fig. 1. Wavelength response diagram: Ge [18], InGaAs [18], [19], Si [18], and bSi [20] image sensors QE comparison.

is problematic because relevant features lay between the interfaces. Traditional methods for investigating the quality of the bonded interfaces include postbond X-ray inspection [12], [13], [14] and through-silicon infrared (IR) microscopy, which exploits silicon transparency at wavelengths longer than 1 μm. Through-silicon substrate imaging is beneficial for semiconductor components alignment evaluation and monitoring the bonding process in real time [15], [16].

The most typical image sensor type used for modern through-silicon IR microscopy is InGaAs or Ge-based camera, which allows the detection of longer wavelengths [17], [18], [19], [20]. Unfortunately, these types of cameras have a number of disadvantages, the most significant of which are rather limited resolution and relatively high price compared with shorter wavelength cameras utilizing silicon-based charge-coupled device (CCD) or CMOS technology. Typical parameters of commercially available cameras are: resolution of 640 $\times$ 512 with 15 $\times$ 15 μm pixel pitch for InGaAs and 640 $\times$ 480 with 10 $\times$ 10 μm pitch for Ge sensors. In addition, those types of cameras often require additional cooling devices [air fan, liquid cooling, and thermoelectric cooling (TEC)] for reproducible acquisition during precise metrology measurements.

A comparison of wavelength response, i.e., quantum efficiency (QE) for conventional Si-CMOS [18], Ge [18], InGaAs [18], [19], and a so-called black silicon (bSi) CMOS-based [20] image sensors is presented in Fig. 1. As it can be seen, at a wavelength range near the 930 nm, bSi image sensor has a sensitivity level comparable to InGaAs image sensor and up to five times higher than that of conventional Si image sensor at wavelengths longer than 1 μm [20], which allows image detection at wavelengths beyond silicon transparence window enabling imaging through silicon substrates. This enhanced response of bSi is due to the light-trapping effect of surface morphology and energy level of dopants: the surface turns deep black being structured by micro–nanospikes, which significantly reduces light reflection and enhancing optoelectronic response. In general, bSi possesses unique optical and electronic properties that are not found in traditional bulk silicon, making it promising candidate material for IR devices [21], [22], [23]. To this end, here, we propose an imaging solution based on nanostructured bSi CMOS sensors.

Besides studying the use of bSi camera for wafer level packaging, we report the development, characterization, and implementation of a cost-effective machine vision solution for through-silicon IR microscopy. The system is based on commercially available optical components and a camera having enhanced long wavelength response, which is based on nanostructured bSi surface. We demonstrate the ability of through-silicon vision for one- and two-layered silicon PIC samples.

Also, we demonstrate a passive autofocusing subsystem, which uses the image spatial spectrum analysis methods. The proposed machine vision system could be used in photonic integration applications but also to improve wafer bonding and lithographic processes requiring similar solutions.

II. IR Microscope Optical Design

The optical scheme of the IR microscope design is presented in Fig. 2. It is based on a classical reflected light microscope architecture with bottom coaxial illumination. It has two illumination devices—IR light-emitting diode (LED) with a center wavelength of 1100 nm and visible LED with emitting spectra of 400–700 nm, which was added as a pilot beam subsystem to optimize the setting of the microscope working point. Both LEDs are equipped with current driving circuits and aspheric condenser lenses with diffusers in order to achieve uniform illumination of the observation area. The setting of working point is performed using precise linear XYZ-stages. The key feature of this design is the implementation of bSi commercially available SiOnyx XQE-0920 image sensor camera with a pixel size of 5.6 $\times$ 5.6 μm and a resolution of 1280 $\times$ 720 pixels [20]. This solution is cost-effective as the price of bSi-based camera normally is at least 3–5 times lower compared to InGaAs- or Ge-based cameras.

In order to protect the image sensor from possible damage during LAB process, the setup is equipped with optical long-pass filter with a cut-on wavelength of 1000 nm and a damage threshold of 12 kW/cm^2 (0.3 J/cm^2) for continuous wave (CW) (pulsed) mode; this blocks all visible wavelengths and most typical laser illumination at 980 nm used in LAB processes [8], [9], [19].

The wavelength response diagram of IR microscope components and typical LAB source spectrum are presented in Fig. 3. Most of the optical components are in 30-mm cage cube packages, and the interconnections between them are made using standard 1″ (1 in diameter) lens tubes.

The ability of through-silicon vision is obtained by using the bottom illumination source with wavelength corresponding to silicon transparence window (the PIC transmittance spectrum is presented in Fig. 4). The apochromatic near infrared response (NIR) objective has a 10$\times$ magnification, numerical aperture (NA) of 0.26, damage threshold of 0.5 kW/cm^2 (0.2 J/cm^2), and a working distance of 30.5 mm on the top surface of sample under test. After adjusting the focus by using the precise Z-stage, it becomes possible to observe the waveguide structures and surface mount pads of the 15 $\times$ 10 $\times$ 0.65 mm silicon PIC used for evaluation [24], [25], which is necessary for high-precision alignment of semiconductor devices and bonding quality control during photonic integration processes. Moreover, varying the objective focus point, it becomes possible to switch observation point between stacked silicon PICs. Fig. 5 shows the obtained image

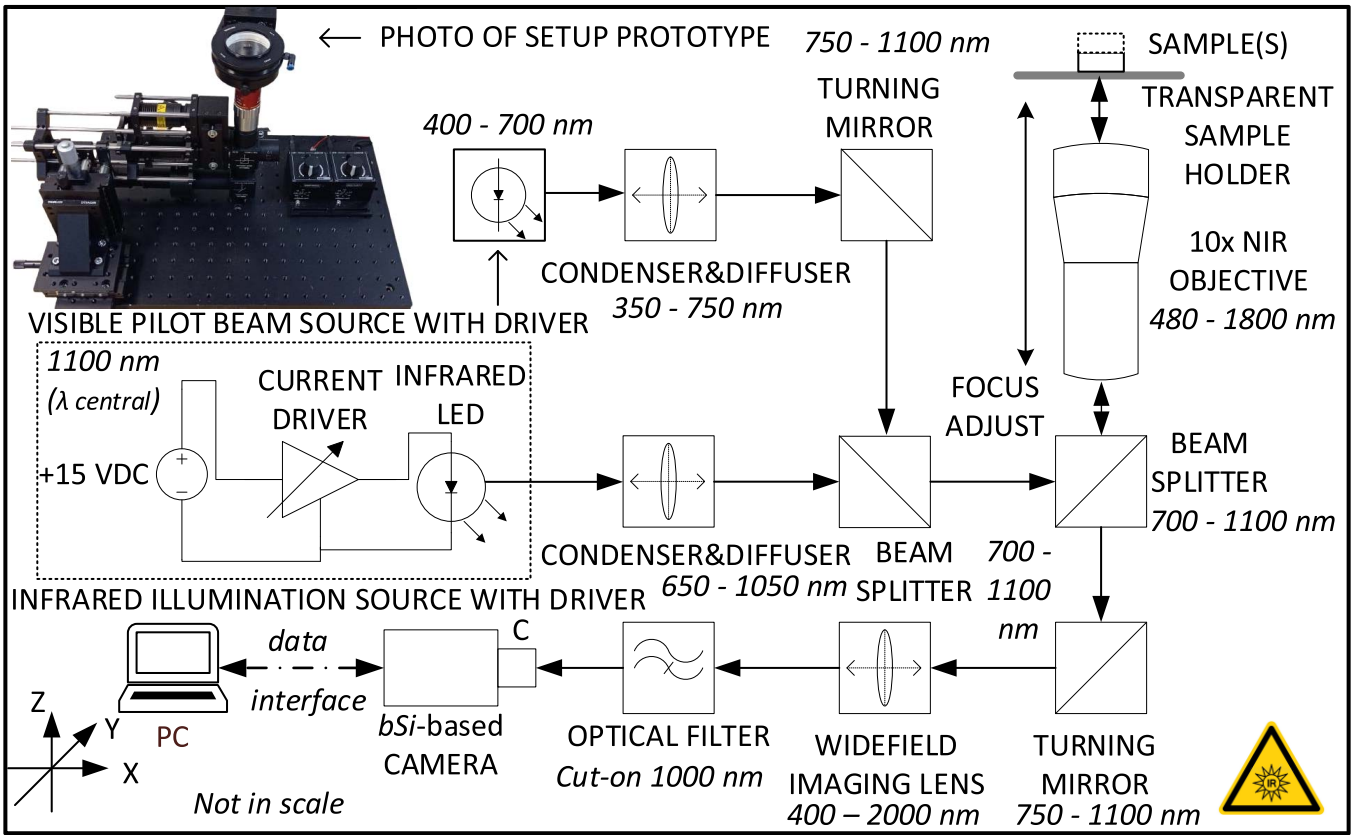

Fig. 2. Photograph and optical scheme of the proposed IR microscope design for through-silicon vision.

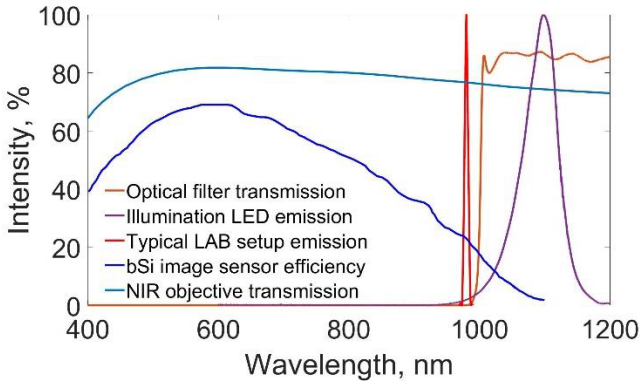

Fig. 3. Wavelength response diagrams: components of the IR microscope proposed design.

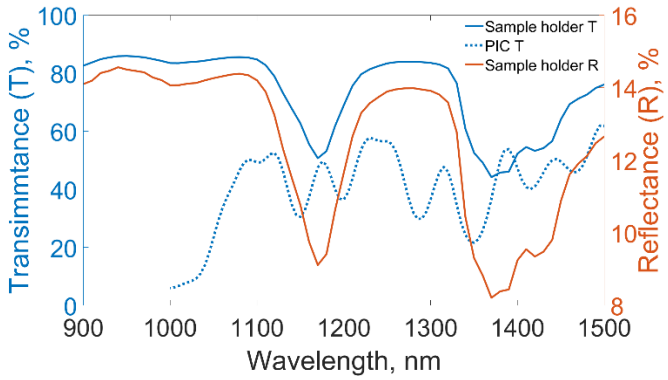

Fig. 4. Transmittance and reflectance data for sample holder transparent layer and PIC sample.

of single-layered silicon PIC top surface. Fig. 6 represents obtained through-silicon images of double-layered silicon structure: first layer (a) and second layer (b) top surfaces.

The bias of the IR LED was set in order to keep the brightness of the highly reflective component images (e.g., golden surface mount pads) in the range of 90%–95% of image sensor brightness saturation limit to obtain the maximum possible image contrast.

The contrast of images along the center line of the component was above 19% for the single-layered PIC, above 12% for the bottom and above 8% for the top layer of the double-layered PIC; the waveguide structures, surface topology elements, and alignment markers are distinguishable in each of considered cases and could be recognized by image processing algorithms, which can give input and feedback for the selection of region of interest and a variety of self-alignment techniques [19], [26]. The image contrast was evaluated according to the following equation [27]:

$$\text{Contrast}(\%) = \frac{(I_{\max} - I_{\min})}{(I_{\max} + I_{\min})} \cdot 100\% \quad (1)$$

where $I_{\max}$ is the image maximum brightness value (digits) and $I_{\min}$ is the image minimum brightness value (digits).

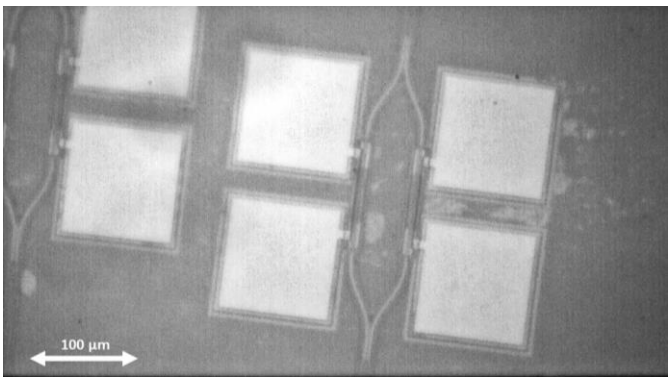

Fig. 5. Single-layered silicon PIC top surface image (through Si).

The contrast rate obtained on real PIC sample pictures confirms that the proposed IR microscope works for the test scenarios. The ability of vision through several layers of silicon is highly beneficial for 2.5-D and 3-D integration processes and bonding quality inspection [4], [28], [29].

III. IR Microscope Optical Characterization

The characterization of the proposed optical circuit in terms of resolution and scale factor is made through the measurement and analysis of the modulation transfer function (MTF [27], [30]) using 1″ positive and negative 1951 USAF test targets (United States Air Forces MIL-STD-150A standard of 1951, test pattern groups 2–7 with element size from 125 down to 2.19 μm) both for sagittal and tangential orientation. The experiment was carried out involving a transparent sample holder (chuck) for test targets placement. In the prototype of the sample holder for through-silicon microscopy applications (e.g., components/wafers entrance control or postbond quality inspection [15], [16], [17], [19]), a laser-cut 3-mm-thick polymethyl methacrylate (PMMA) plastic sheet is used as a transparent layer. Its transmittance and reflectance spectrums, as well as the transmittance spectrum of the used PIC sample, are presented in Fig. 4. The data were obtained by using the spectrophotometer setup. For LAB applications in order to avoid heat damage, melting, and deformation of the surface, it is necessary to use AR-coated materials with high light durability, such as Sapphire [19] or Borofloat glass, which has wide transmittance spectrum up to wavelengths of more than 2.5 μm [31]. These should be preferably processed by waterjet cutting technique as it does not produce a heat affected zone and therefore, the material is free from thermal and deformation stresses, leading to fine and clean cut [32]. The test target was placed on the sample holder above the IR microscope objective as shown in Fig. 2, and after adjusting the focus with a precise Z-stage, an image of each test pattern groups was taken.

The contrast of each taken image across the centerline of the element was subsequently calculated using (1). The bias of the illumination IR LED has been preset to keep the brightness of the largest element images in the range of 90%–95% of the saturation limit to obtain the maximum possible contrast and should not be changed during the experiment.

The experimental results of the MTF analysis are presented in Fig. 7. As it can be seen, even the smallest test patterns of group 7 with an element size of 2.19 μm have a contrast rate near 5% both for sagittal and tangential orientation of positive and negative test targets (average contrast 5.3%), which satisfies minimal contrast of 3%–5% for determination of optical system limiting resolution [27]. Thus, the proposed optical system is suitable for observing elements with dimensions down to 2 μm, which is close to the theoretical diffraction limit and corresponds to the dimensions of optical waveguide structures on the PIC surface. The evaluation of scale factor is proceeded by the same test target type. The width of the element with highest contrast rate (element 1 of group 2) is 125 μm, which corresponds to the element image width of 206 pixels for sagittal orientation and 212 pixels for tangential orientation of the negative test target, and 213 pixels for sagittal orientation and 209 pixels for tangential orientation of the positive test target. All values were estimated at 90% level of maximum image intensity to reduce the intensity ripple effects. Thus, assuming the square shape of image sensor elements (5.6 $\times$ 5.6 μm), the observed physical object of 125 μm on the average corresponds to the image of 210 pixels. This gives the scale factor of 0.6 μm per pixel for the optical system. Accordingly, the microscope observation area is 768 $\times$ 432 μm. This scale factor is needed for measurement purposes during semiconductor components alignment and bonding quality inspection.

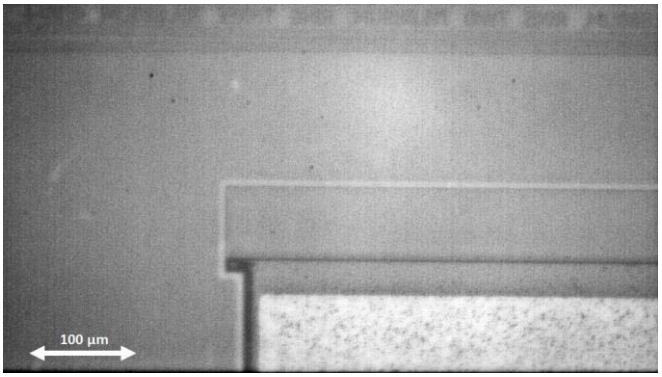

(a)

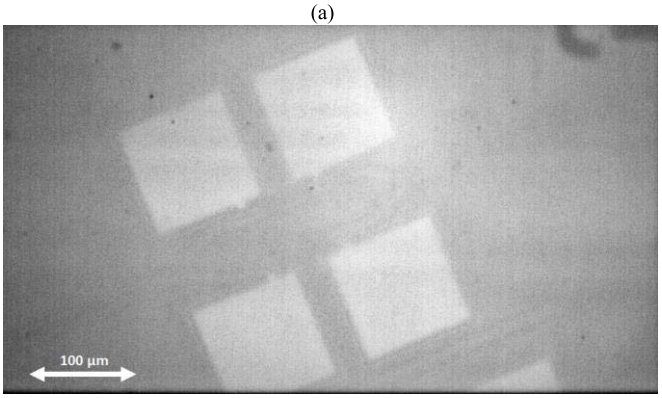

(b)

Fig. 6. Images of double-layered stacked silicon PIC structure: (a) bottom layer and (b) top layer surfaces (through Si). The images were taken at the same *xy* position.

IV. Passive Autofocus Subsystem

Due to the usage of the objective with 10$\times$ magnification and NA of 0.26, and therefore, narrow depth of focus, the

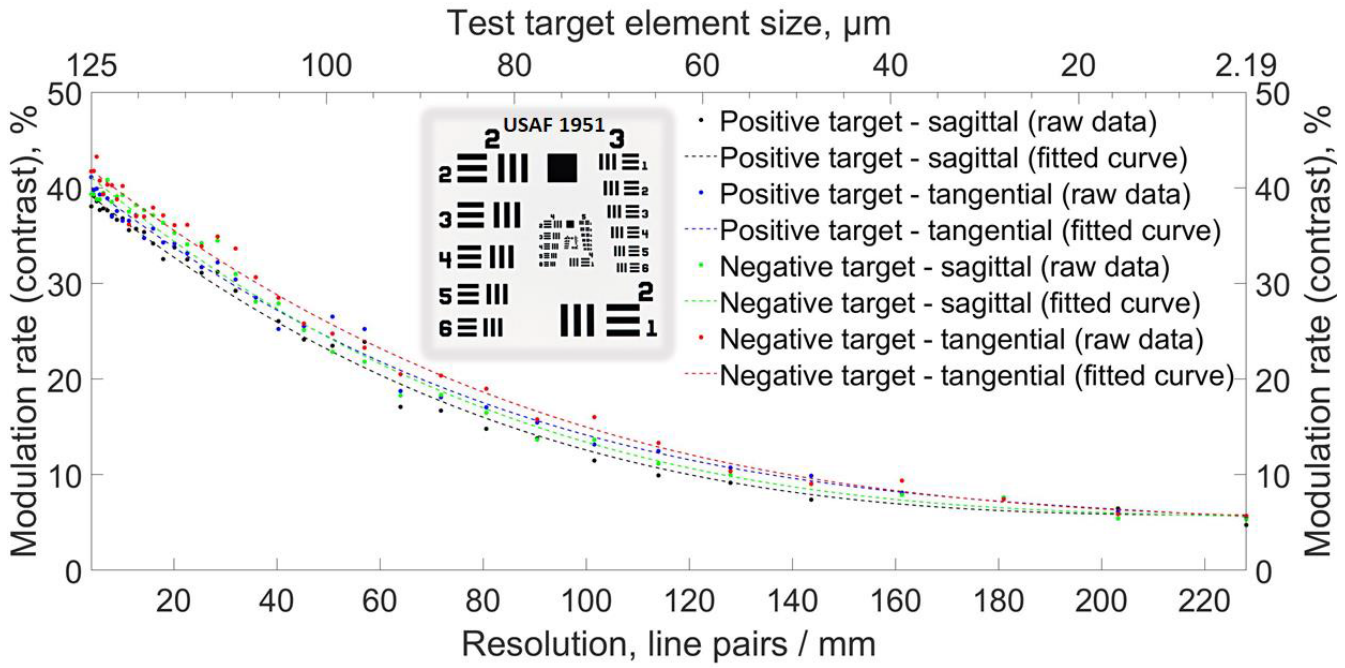

Fig. 7. Results of MTF evaluation using USAF-1951 target (test pattern groups 2–7).

proposed IR microscope design is very sensitive to variations of focal distance—the image easily becomes defocused due to vibrations and hit impacts. Thus, the system should be mounted on a solid rigid basis with the use of properly designed vibration isolation system [33].

For the ease of obtaining the best in-focus images, the IR microscope was equipped with a passive autofocus subsystem, which is based on the numerical analysis of a 2-D amplitude spectrum of the image [34]. The passive autofocusing is preferable as such subsystems do not require any additional optical signals besides the illumination light; it is based on analyzing the received image that is then used for commanding a motorized linear stage to adjust the working point. This avoids complicated designs, avoiding the need to use additional light sources or sensors [34].

To find the optimal focus point, a scanning along the z-axis using motorized stage is performed while taking images on each scanning step, using global search scanning method [34]. The image arrays $f(x, y)$ with resolution of M by N ($x = 0, 1, 2, \ldots, M-1$ and $y = 0, 1, 2, \ldots, N-1$) pixels are then analyzed by using as a criterion the overall sum S of the components of the direct 2-D fast discrete Fourier transform as a merit of image in-focus degree, i.e., by calculating the sum of the amplitude elements of the spatial frequency spectrum according to the following equation [34]:

$$S = \sum_{u=0}^{M} \sum_{v=0}^{N} \left| \frac{1}{MN} \sum_{u=0}^{M-1} \sum_{v=0}^{N-1} f(x, y) e^{-i2\pi \left(\frac{ux}{M} + \frac{uy}{N}\right)} \right| \qquad (2)$$

where $u = 0, 1, 2, \ldots, M-1$ and $v = 0, 1, 2, \ldots, N-1$.

Finally, the optimal focusing point is then determined by the largest width of the spectrum as the best in-focus image is the most detailed. Although Fourier analysis requires significant computing power, the key advantage of this method is that it avoids using any sophisticated image processing algorithms, such as object recognition, edge detection, global or local variance analysis, contrast or gradient estimation, derivative, histogram or correlation analysis, as well as the usage of any additional hardware [26], [35], [36], [37]. The only merit for finding the best in-focus image is the maximum value of the 2-D Fourier transform components sum. In our case, using a personal computer (×64-based CPU at 2.21 GHz with 16-GB RAM), this method can be easily implemented, e.g., by standard means of MATLAB environment. After scanning, the motorized stage should be returned to the position, which corresponds to the point, where image of desired object of interest contains maximum sum of spectral components—this is the optimal focus point. In case there are several peaks resulting from the analysis, the object of interest should be chosen manually. The ability of switching between several peaks for changing the best in-focus point between different layers of the stack is beneficial for 2.5-D and 3-D photonic integration processes and bonding quality inspection [4], [28], [29]. This approach could also be used for estimating the layer thickness in multilayer silicon structure with resolution limited only by stage minimum traveling step.

The scheme of the measuring setup is presented in Fig. 8 (for simplicity, the IR microscope (Fig. 2) is depicted as a solid camera). The experiment is carried out as follows: preliminary working distance is preset near the transparent surface of a sample holder. Then, the scanning with a step of 20 μm along the z-axis is initialized. The spectrum components sum is calculated for each step. The illumination IR LED bias has been preset to keep the brightness of the largest element images in the range of 90%–95% of image sensor brightness saturation limit to obtain the maximum possible contrast, and it should not be change during the experiment. As all the images

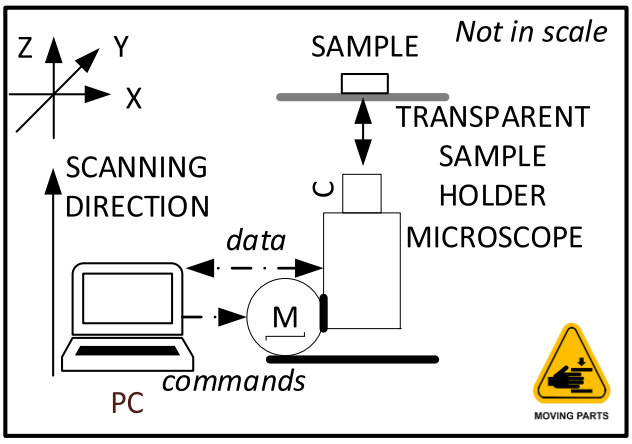

Fig. 8. Fourier-based autofocus subsystem evaluation setup.

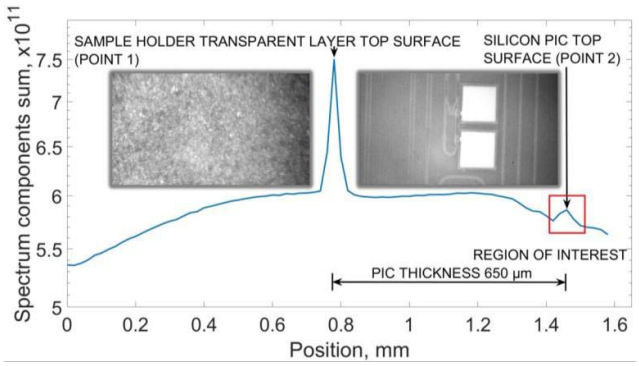

Fig. 9. Fourier-based autofocus subsystem experimental data.

in a series are taken under equal conditions, there is no need for calibration of the autofocusing subsystem.

The experimental data are presented in Fig. 9. As it can be seen, the local maxima of the values of the spectrum components sum correspond to the best in-focus images—point 1 is related to the top surface of transparent layer and point 2 is related to the desired object of interest—the top surface of silicon PIC. The significant difference in the sum of the spectral components values for transparent layer and PIC can be explained: the PIC is based on double-side polished piece of silicon substrate, and its surface roughness (measured value is in the range of nm units; dimensions of observable surface topology elements—from units to hundreds of μm) is much lower than that of the PMMA sheet, which contains a lot of surface texture features in the range of tenths and units of μm depending on processing quality [38], [39], observable under 10× magnification.

The average execution time for each single image analysis is 25 ms. The 1.6-mm range average scanning time is 4.5 s, and it consists of obtaining and receiving an image from camera via data exchange interface, data acquisition, its analysis, and moving the electrical motor by 20 μm at one step. The region of interest (Fig. 9) average scanning time is 250 ms. The performance analysis indicates that the implemented autofocusing method compares favorably with other known autofocusing algorithms with execution time from 2 to 700 ms per frame [34]. The subsystem performance can be further increased by the implementation of improved scanning (search) techniques, shortening the scanning distance, or narrowing the image area to focus [35], [36], [37]. These approaches reduce the number of taken images and the amount of data to analyze.

It should also be mentioned that small elements (surface scratches, visible particles, defects, etc.) with dimensions comparable to the minimum observable object range being focusing on tend to generate a sufficiently wide spatial spectrum to affect the operation of any Fourier-based autofocus approach. Thus, it is an additional reason to maintain cleanliness and caution when working with the equipment under normal conditions. However, those limitations can be easily overcome when using the proposed design in photonic integration processes as they impose serious demands on the cleanliness of media, surfaces, materials, and tools used, requiring operation in cleanroom environment.

Thus, the implementation of the described passive method of finding and maintaining of best in-focus point is valuable for using the proposed IR microscope design in a large variety of research and assembly setups [17], [19].

V. Conclusion

A cost-effective design of an IR microscope with a coaxial bottom illumination architecture based on a commercial nanoroughened bSi surface image sensor camera was demonstrated. The ability of through-silicon vision was confirmed for single- and double-layer stacked silicon PIC structures. The ability of switching the observation point between layers of a multilayer silicon structure is beneficial for 2.5-D and 3-D integration processes and bonding quality inspection. Optical characterization of the proposed design using MTF analysis confirmed the ability of observing objects with dimensions down to 2 μm, which is close to the theoretical diffraction limit. Furthermore, this resolution also corresponds to the dimensions of optical waveguide structures on PICs and satisfies the needs of assessing the components alignment and bonding quality.

Also, we report implementation results of a passive autofocus subsystem, based on the numerical analysis of 2-D spatial spectrum of the image for through-silicon IR microscopy. The best in-focus point is determined by the largest width of the spatial spectrum, as the focused image is the most detailed. Using this dependence, it is possible to formulate a criterion of the degree of focusing of the image obtained by the IR microscope—the greater the overall sum of the amplitudes of all harmonics of the spatial spectrum, the better the obtained image is focused. The performance attained indicates that the implemented autofocusing method compares favorably with other known autofocusing algorithms. Thus, by using this feature in tandem with precise motorized Z-stage, an effective subsystem for setting and maintaining the optimal focus point could be created. This method can be easily implemented, e.g., by standard means of MATLAB environment. Also, similar approach could be used for the estimation of the layer thickness in multilayer silicon structure with resolution limited only by the minimum traveling step of the stage.

The machine vision system demonstrated could be used in photonic integration processes and other through-silicon

vision-related applications and may be implemented to a large variety of research and assembly setups.

ACKNOWLEDGMENT

The authors are grateful to FabLab Tampere (Tampere, Finland) Team and personally to Mika Kiirikki, Riku Koskinen, Ilkka Hirvonen, Antti Tukiainen, and Bengt-Olof Holmström from Tampere University, Tampere, Finland, for their invaluable help with prototyping of the proposed design. They declare that the research was conducted in the absence of any commercial or financial relationships that could be construed as a potential conflict of interest. The funders had no role in the design of the study; in the collection, analyses, or interpretation of data; in the writing of this article, or in the decision to publish the results.

REFERENCES

[1] J. H. Lau, "Recent advances and trends in advanced packaging," *IEEE Trans. Compon., Packag., Manuf. Technol.*, vol. 12, no. 2, pp. 228–252, Feb. 2022, doi: 10.1109/TCPMT.2022.3144461.

[2] P. Kaur, A. Boes, G. Ren, T. G. Nguyen, G. Roelkens, and A. Mitchell, "Hybrid and heterogeneous photonic integration," *APL Photon.*, vol. 6, no. 6, Jun. 2021, Art. no. 061102, doi: 10.1063/5.0052700.

[3] N. Margalit, C. Xiang, S. M. Bowers, A. Bjorlin, R. Blum, and J. E. Bowers, "Perspective on the future of silicon photonics and electronics," *Appl. Phys. Lett.*, vol. 118, no. 22, May 2021, Art. no. 220501, doi: 10.1063/5.0050117.

[4] D. Liang and J. E. Bowers, "Recent progress in heterogeneous III–V-on-silicon photonic integration," *Light, Adv. Manuf.*, vol. 2, no. 1, pp. 1–25, 2021, doi: 10.37188/lam.2021.005.

[5] B. Corbett, R. Loi, W. Zhou, D. Liu, and Z. Ma, "Transfer print techniques for heterogeneous integration of photonic components," *Prog. Quantum Electron.*, vol. 52, pp. 1–17, Mar. 2017, doi: 10.1016/j.pquantelec.2017.01.001.

[6] M. Theurer et al., "Flip-chip integration of InP to SiN photonic integrated circuits," *J. Lightw. Technol.*, vol. 38, no. 9, pp. 2630–2636, May 1, 2020, doi: 10.1109/jlt.2020.2972065.

[7] N. Zia et al., "Hybrid silicon photonics DBR laser based on flip-chip integration of GaSb amplifiers and μm-scale SOI waveguides," *Opt. Exp.*, vol. 30, no. 14, Jun. 2022, Art. no. 24995, doi: 10.1364/oe.460883.

[8] Y. M. Jang, Y. Kim, and S.-H. Choa, "Development and optimization of the laser-assisted bonding process for a flip chip package," *Microsyst. Technol.*, vol. 26, no. 3, pp. 1043–1054, Sep. 2019, doi: 10.1007/s00542-019-04624-8.

[9] M. Gim, C. Kim, S. Na, D. Ryu, K. Park, and J. Kim, "High-performance flip chip bonding mechanism study with laser assisted bonding," in *Proc. IEEE 70th Electron. Compon. Technol. Conf. (ECTC)*, Jun. 2020, pp. 1025–1030, doi: 10.1109/ECTC32862.2020.00166.

[10] M. Mastrangeli, Q. Zhou, V. Sariola, and P. Lambert, "Surface tension-driven self-alignment," *Soft Matter.*, vol. 13, no. 2, pp. 304–327, 2017, doi: 10.1039/c6sm02078j.

[11] K.-S. Choi et al., "Development of digital signage modules composed of mini-LEDs using laser-assisted bonding (LAB) technology," in *Proc. IEEE 70th Electron. Compon. Technol. Conf. (ECTC)*, Jun. 2020, pp. 1031–1036, doi: 10.1109/ECTC32862.2020.00167.

[12] J. Joo, Y.-S. Eom, K.-S. Jang, G.-M. Choi, and K.-S. Choi, "Development of bonding process for flexible devices with fine-pitch interconnection using anisotropic solder paste and laser-assisted bonding technology," in *Proc. IEEE 70th Electron. Compon. Technol. Conf. (ECTC)*, Jun. 2020, pp. 1309–1314, doi: 10.1109/ECTC32862.2020.00207.

[13] C.-Y. Chen, I. Hsu, S. Lin, D. Park, and M.-C. Hsieh, "Laser assisted bonding technology enabling fine bump pitch in flip chip package assembly," in *Proc. 7th Electron. Syst.-Integr. Technol. Conf. (ESTC)*, Sep. 2018, pp. 1–6, doi: 10.1109/ESTC.2018.8546345.

[14] S. Bao et al., "A review of silicon-based wafer bonding processes, an approach to realize the monolithic integration of Si-CMOS and III–V-on-Si wafers," *J. Semicond.*, vol. 42, no. 2, Feb. 2021, Art. no. 023106, doi: 10.1088/1674-4926/42/2/023106.

[15] J.-W. Nah, Y. Martin, S. Kamlapurkar, S. Engelmann, R. L. Bruce, and T. Barwicz, "Flip chip assembly with sub-micron 3D re-alignment via solder surface tension," in *Proc. IEEE 65th Electron. Compon. Technol. Conf. (ECTC)*, May 2015, pp. 35–40, doi: 10.1109/ECTC.2015.7159568.

[16] Y. Martin, J.-W. Nah, S. Kamlapurkar, S. Engelmann, and T. Barwicz, "Toward high-yield 3D self-alignment of flip-chip assemblies via solder surface tension," in *Proc. IEEE 66th Electron. Compon. Technol. Conf. (ECTC)*, May 2016, pp. 588–594, doi: 10.1109/ECTC.2016.239.

[17] G. Böttger, D. Weber, F. Scholz, H. Schröder, M. Schneider-Ramelow, and K.-D. Lang, "Fully automated hybrid diode laser assembly using high precision active alignment," *Proc. SPIE*, vol. 9730, Apr. 2016, Art. no. 97300E, doi: 10.1117/12.2214718.

[18] D. Hobbs et al., "Astro2020 activity, project of state of the profession consideration (APC) white paper: All-sky near infrared space astrometry. State of the profession considerations: Development of scanning NIR detectors for astronomy," 2019, *arXiv:1907.05191*.

[19] *FiconTEC Webinars FiconTEC Service (Sub-μm Through-Silicon Alignment)*. ficonTEC. Accessed: Feb. 16, 2022. [Online]. Available: https://www.ficontec.com/webinar/

[20] M. U. Pralle, C. Vineis, C. Palsule, J. Jiang, and J. E. Carey, "Extending black silicon imaging to backside illumination," *Proc. SPIE*, vol. 9819, May 2016, Art. no. 981904, doi: 10.1117/12.2223063.

[21] Q. Tan, F. Lu, C. Xue, W. Zhang, L. Lin, and J. Xiong, "Nano-fabrication methods and novel applications of black silicon," *Sens. Actuators A, Phys.*, vol. 295, pp. 560–573, Aug. 2019, doi: 10.1016/j.sna.2019.04.044.

[22] J. Lv, T. Zhang, P. Zhang, Y. Zhao, and S. Li, "Review application of nanostructured black silicon," *Nanosc. Res. Lett.*, vol. 13, no. 1, pp. 1–10, Apr. 2018, doi: 10.1186/s11671-018-2523-4.

[23] M. U. Pralle et al., "Black silicon enhanced photodetectors: A path to IR CMOS," *Proc. SPIE*, vol. 7660, Apr. 2010, Art. no. 76600N, doi: 10.1117/12.849683.

[24] T. Aalto et al., "Open-access 3-μm SOI waveguide platform for dense photonic integrated circuits," *IEEE J. Sel. Topics Quantum Electron.*, vol. 25, no. 5, pp. 1–9, Sep. 2019, doi: 10.1109/jstqe.2019.2908551.

[25] S.-P. Ojanen et al., "GaSb diode lasers tunable around 2.6 μm using silicon photonics resonators or external diffractive gratings," *Appl. Phys. Lett.*, vol. 116, no. 8, Feb. 2020, Art. no. 081105, doi: 10.1063/1.5140062.

[26] A. A. Makarenko, A. D. Makarov, A. A. Vlasov, and E. A. Motorin, "Application of digital image processing for selection of ROI on the image," *Radio Ind.*, no. 2, pp. 25–28, Jan. 2017, doi: 10.21778/2413-9599-2017-2-25-28.

[27] N. Menn, *Practical Optics*. Amsterdam, The Netherlands: Elsevier, 2004, pp. 66–70.

[28] X. Yang et al., "2.5D Optoelectronic Integration for 400G (8×56Gbps) CPO-based optical interconnects," in *Proc. Asia Commun. Photon. Conf.*, Oct. 2021, pp. 1–3, doi: 10.1364/ACPC.2021.T2D.2.

[29] W. A. Braganca, Y. Eom, K. Jang, S. H. Moon, H. Bae, and K. Choi, "Collective laser-assisted bonding process for 3D TSV integration with NCP," *ETRI J.*, vol. 41, no. 3, pp. 396–407, Apr. 2019, doi: 10.4218/etrij.2018-0171.

[30] *Introduction to Modulation Transfer Function | Edmund Optics*. Accessed: Jan. 18, 2022. [Online]. Available: www.edmundoptics.com.https://www.edmundoptics.com/knowledge-center/application-notes/optics/introduction-to-modulation-transfer-function/

[31] R. Witte, H. J. Herfurth, and I. Bauer, "Microjoining of dissimilar materials for optoelectronic and biomedical applications," *Proc. SPIE*, vol. 4979, pp. 226–233, Jan. 2003, doi: 10.1117/12.478282.

[32] S. Nisar, L. Li, and M. A. Sheikh, "Laser glass cutting techniques—A review," *J. Laser Appl.*, vol. 25, no. 4, Aug. 2013, Art. no. 042010, doi: 10.2351/1.4807895.

[33] A. A. Vlasov et al., "Development of the passive vibroacoustic isolation system for the path matched differential interferometry based fiber-optic sensors," *Opt. Fiber Technol.*, vol. 57, Jul. 2020, Art. no. 102241, doi: 10.1016/j.yofte.2020.102241.

[34] A. A. Makarenko and L. A. Vinokurov, "Application of digital image processing for autofocusing system construction," *Radio Ind. (Russia)*, vol. 30, no. 2, pp. 69–79, Jun. 2020, doi: 10.21778/2413-9599-2020-30-2-69-79.

[35] C.-N. Nguyen, K. Ohara, T. Takubo, Y. Mae, and T. Arai, "High-speed autofocusing of multisized microobjects," in *Proc. IEEE Int. Conf. Autom. Sci. Eng. (CASE)*, Aug. 2012, pp. 34–39, doi: 10.1109/CoASE.2012.6386495.

[36] N. N. K. Chern, P. A. Neow, and M. H. Ang, "Practical issues in pixel-based autofocusing for machine vision," in *Proc. ICRA. IEEE Int. Conf. Robot. Autom.*, May 2001, pp. 2791–2796, doi: 10.1109/ROBOT.2001.933045.

[37] J. Alvarez-Borrego, "Fast autofocus algorithm for automated microscopes," *Opt. Eng.*, vol. 44, no. 6, Jun. 2005, Art. no. 063601, doi: 10.1117/1.1925119.

[38] M. A. Abuzar et al., "Evaluating surface roughness of a polyamide denture base material in comparison with poly (methyl methacrylate)," *J. Oral Sci.*, vol. 52, no. 4, pp. 577–581, 2010, doi: 10.2334/josnusd.52.577.

[39] Y. Huang, S. Liu, W. Yang, and C. Yu, "Surface roughness analysis and improvement of PMMA-based microfluidic chip chambers by CO_2 laser cutting," *Appl. Surf. Sci.*, vol. 256, no. 6, pp. 1675–1678, Jan. 2010, doi: 10.1016/j.apsusc.2009.09.092.

Aleksandr Andreevich Vlasov was born in Lviv, Ukraine. He received the B.Eng. degree in telecommunications, the M.Eng. degree in optical systems and communication networks, and the Ph.D. degree in engineering (optical and optoelectronic devices and complexes) from ITMO University, Saint Petersburg, Russia, in 2014, 2016, and 2020, respectively. His dissertation research was related to various methods of fiber-optical interferometers and fiber lasers cavities desensitization to environmental noise and vibration impacts.

Having overall diverse research and development experience of more than ten years on positions from Laboratory Assistant to Research Engineer with ITMO University, he joined the Optoelectronics Research Centre, Tampere University, Tampere, Finland, in March 2021, as a Post-Doctoral Research Fellow. He has authored or coauthored more than 15 scientific articles. His current research interests include semiconductor packaging and bonding technologies, silicon photonics, and optoelectronic instrumentation.

Alp Eren Aydin was born in Bursa, Turkey. He received the B.Eng. degree in electrical and electronics engineering from Akdeniz University, Antalya, Turkey, in 2016, and the M.Sc. degree in electrical and electronics engineering from Bursa Technical University, Bursa, in 2020; and he has graduated from an EMJMD triple degree program from KU Leuven, Leuven, Belgium; the University of Eastern Finland, Joensuu, Finland; and Toyohashi University of Technology, Toyohashi, Japan.

He took part in ERASMUS Exchange Program in photonics at the University of Eastern Finland, in 2018. He has held a research and development position at the Ermaksan Optoelectronics Research Centre, Bursa. He was an Electrical Engineer with Ayel Yapi Denetim, Bursa. He has been working as a Research Assistant with the Optoelectronics Research Centre, Tampere University, Tampere, Finland, since 2021. His research interests include silicon photonics, hybrid and heterogeneous photonic integration, micro-optics assemblies, and numerical simulation.

Topi Uusitalo received the Ph.D. degree in engineering physics from the Tampere University of Technology, Tampere, Finland, in 2018.

He is currently working as a Post-Doctoral Researcher with the Optoelectronics Research Centre, Tampere University, Tampere, in research areas in high power edge emitting laser diodes, vertical cavity surface-emitting lasers (VCSELs), from device design to characterization. He has authored or coauthored more than 20 scientific works.

Jukka Viheriälä is currently a Senior Scientist with the Faculty of Engineering and Natural Sciences, Tampere University, Tampere, Finland, responsible for micro- and nanofabrication, where his research interests are linked to the development of novel optoelectronic devices at the Optoelectronics Research Centre. He has more than 15 years of experience as a Researcher, with particular focus on optoelectronics device fabrication, testing, and characterization. Most recently, he was responsible for the nanoimprint lithography capabilities for laser diode processing and contributed to obtaining several pioneering results in this area. He has also developed optoelectronics devices tailored for hybrid integration to silicon photonics technology and contributes to progress in high-power single-frequency diode lasers and mid-infrared (IR) laser and gain chips. Besides his academic work, he has been active in commercialization of research at the Optoelectronics Research Centre in various roles in technical and business development. He has authored or coauthored more than 100 scientific articles.

Mircea Guina (Member, IEEE) received the Ph.D. degree in physics from the Tampere University of Technology, Tampere, Finland, in 2002.

Since 2008, he has been a Professor of Semiconductor Technology (Optoelectronics) and leads the Optoelectronics Research Centre Team, a research group part of the Faculty of Engineering and Natural Sciences, Tampere University, Tampere. He is also the Co-Founder and the Chairperson of three start-ups related to laser technologies (Vexlum Oy, Reflekron Oy, and Picophotonics Oy, Tampere, Finland). He has an outstanding track record in initiating and leading large-scale research projects extending from basic science to technology transfer. He has authored more than 200 journal articles and nine book chapters, has given more than 40 invited talks at major international conferences, and holds four international patents. He conducts research on several major topics including molecular beam epitaxy of novel optoelectronic compounds, development of semiconductor lasers and high-efficiency solar cells, photonic integration, and use of lasers in medicine, light detection and ranging (LIDAR), and sensing.

Dr. Guina was a recipient of the European Research Council (ERC) Advanced Grant for the development of high-efficiency solar cell technology (AMETIST). He was awarded the Optical Society (OSA) Fellow and the Society of Photo-Optical Instrumentation Engineers (SPIE) Fellow distinctions for his work on optoelectronics and laser technologies. He is a Topical Editor of the *Optics Letters* journal and the *Journal of European Optical Society*.